Rough-surface gravity current flows

W.D. Peters [1] and J.E.S. Venart [2]

[1] Department of Engineering, University of Prince Edward Island, Charlottetown, Prince Edward Island, Canada
[2] Department of Mechanical Engineering, University of New Brunswick, Fredericton, New Brunswick, Canada

ABSTRACT

A quantitative, full-field planar visualization technique was developed and successfully used to assess the flow dynamics and mixing behaviour of gravity current heads flowing over rough surfaces. Small-scale saltwater modelling, laser-induced fluorescence (LIF) and digital image processing were combined to analyze the roughness effects on the downstream spread and dilution rates of continuous source, parallel channel gravity current flows moving over beam-roughened surfaces. The work was completed in three phases: 1) the development of the modelling, visualization and analysis techniques; 2) the validation of these techniques using published results from well-documented, smooth-surface flow studies and 3) the evaluation of how well the published smooth-surface flow theory extends to rough-surface flows. This paper will focus on the first of these three phases, describing the LIF visualization and analysis techniques used. Extension of smooth-surface theory to the rough-surface gravity current flows considered here will be discussed.

Three series of tests, with source fluid density excesses of 1, 3 and 5%, were performed. The source injection flow rates were 10.3, 10.6 and 10.8 cm^2/s, respectively, which resulted in source buoyancy fluxes of 101, 312 and 530 cm^3/s^3, respectively. Five surface roughness conditions were examined for each series of tests, yielding a total of fifteen tests. These included a smooth-surface condition for each test series, providing a base case against which the rough-surface flow results were compared. The roughness arrays consisted of square-beam elements, 6, 13, 19 and 25 mm on a side, placed perpendicularly to the flow in a repeated array down the length of the water channel.

The experimental facility and techniques developed can successfully provide full-field, planar images of rough-surface gravity current flows to facilitate qualitative and quantitative study of the downstream spread rate and mixing. An image of a gravity current flowing over a rough surface to the left is given in Figure 1. The darker regions internal to the head represent pockets of lighter ambient fluid entrained into the head from the roughness element spaces below. Results from the smooth-surface test cases generally agree very well with the accepted theory and observations in terms of structure, flow dynamics and mixing behaviour. It was demonstrated that the assumption of no mixing between the current head and the ambient fluid, adopted by the constant advance velocity model, is acceptable for smooth-surface flows only. Modifications to this model were developed to allow its extension to rough-surface flows in which larger shear stresses and increased internal head mixing exist. The results of this work should contribute to the on-going development and improvement of predictive models for heavier-than-air-gas (HTAG) dispersions over rough-surfaces.

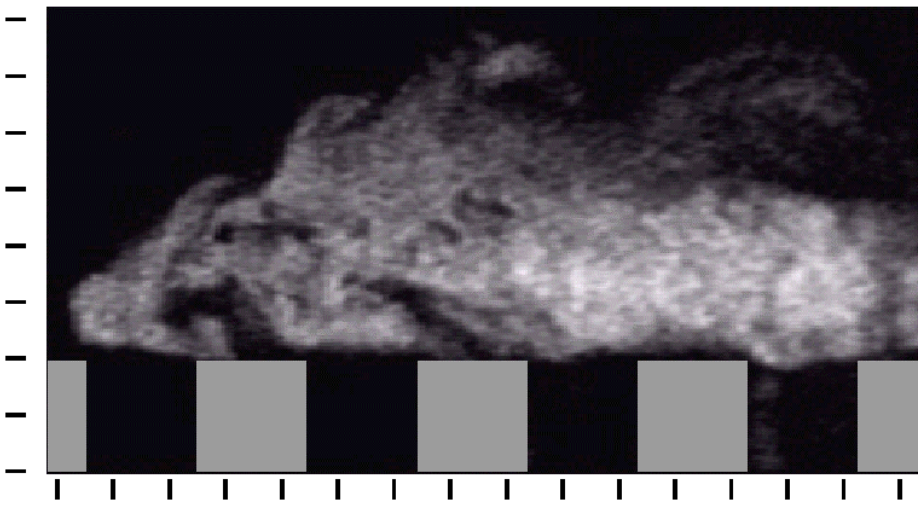

Fig. 1. Image showing internal mixing regions in a gravity current head with a 1% source fluid density excess f lowing over a 19 mm roughness element array. Scales shown are in 1 cm increments.

1. INTRODUCTION

1.1 Description of a Gravity Current

Gravity currents belong to a class of fluid flows in which buoyant forces, generated by density variations, produce motions predominantly in a direction normal to the gravity vector. This type of flow can be created, for instance, when a heavier fluid is introduced into a reservoir of less dense fluid after which it slumps to the bottom and spreads horizontally as a gravity current. This type of flow is known as a dense gravity current. Similarly, a buoyant free-surface flow can be generated in a fluid into which a lighter fluid is released. Generally, the fluids that form a gravity current are miscible so that mixing between the current and ambient fluids plays a significant role in the flow dynamics.

The primary feature of a dense gravity current, flowing over a smooth surface, is a well-defined raised head formed at the downstream leading edge of a shallower flowing source layer as shown in Figure 2. The leading point of this head exhibits a slightly elevated nose which allows less dense ambient fluid to be overrun by the structure as it advances. Behind the head, a stable and quiescent interface separates the lower source layer from an adjacent layer formed above it. This upper layer consists of an intermediate-density mixed fluid that results from the mixing between the ambient and source fluids within the head.

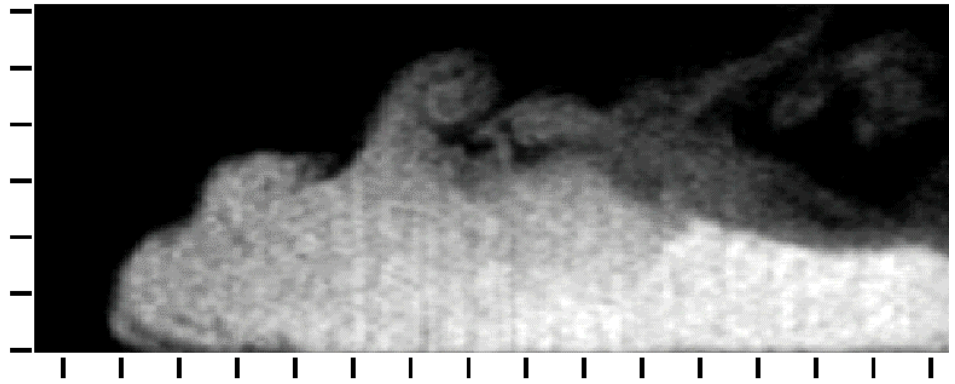

Fig. 2. Image of a typical gravity current head with a 1% source fluid density excess flowing to the left over a smooth surface. Scales shown are in 1 cm increments.

Through evaluation of the spreading and dilution behaviour of the flow, two basic gravity current mixing mechanisms have been defined by the authors' work and that of others found in the published literature. Firstly, Kelvin-Helmholtz instabilities, initiated by velocity and density gradients at the intruding head/ambient fluid interface, lead to mixing along this region. This results in billows and waves that flow up and over the head to settle in the intermediate-density mixed layer behind. Secondly, mixing internal to the head region arises as a layer of lighter ambient fluid is overrun by the advancing head. The velocity shear between this overrun fluid and the current head causes further Kelvin-Helmholtz instabilities at this level. Additionally, this overrun fluid is buoyantly unstable and, thus, Taylor instabilities further contribute to, and perhaps even dominate, the internal head dilution process.

Natural gravity current examples are plentiful. Characterized by large-scale atmospheric movements of relatively cool air, thunderstorm outflows and sea-breeze fronts exhibit classic gravity current behaviour. Fog banks, consisting of fluidized suspensions, and avalanches, created by particulate suspensions of air-borne snow, behave in a similar manner. In the oceans, gravity currents appear as turbidity currents or as salt-water intrusions that can travel long distances up fresh-water rivers. In a man-made world, discharges of waste water and power plant cooling water can significantly alter the rivers and lakes into which they are dumped, as warmer water flows across the surface in the form of a gravity current. Oil, released during an ocean spill, spreads in the form of a gravity current and can result in serious damage to the environment. The transport of combustion products along the ceiling of a burning building and the spread of hazardous heavier-than-air-gases (HTAG) over land are, also, governed by the gravity current flow phenomenon. Information gained through the current authors' work will be applied to the last of these examples - HTAG dispersions.

1.2 Gravity Current Flow Modelling

A large bulk of work exists in the published literature that focusses on the spreading and mixing behaviour of gravity current flows over smooth surfaces. As early as the beginning of the twentieth century, Schmidt (1911) used temperature-induced density differences to create small-scale gravity current flows while studying atmospheric cold fronts. Through his experiments, he was able to demonstrate the effect of Reynolds number, and thus, viscosity, on the flow. He concluded that an upper limit exists for which the level of turbulent mixing in the flow is typical of all flows with Reynolds numbers several orders of magnitude higher than his small-scale flows. This conclusion was later supported by the works of Keulegan (1957, 1958) and Simpson and Britter (1979) using salt-water modelling methods.

The first mathematical treatment of the gravity current flow is attributed to von Kármán (1940). He applied Bernoulli's theorem along streamlines on either side of the interface between the current and ambient fluids to develop an expression for the gravity current advance velocity. In his form, the velocity was a function of the density difference between the two fluids, using the Boussinesq approximation and a reduced gravity term, and a vertical length scale representing the height of the flow. In a normalized form, this expression for velocity is essentially the densimetric Froude number.

Keulegan's work (1957, 1958), also, advanced this Froude number definition of the frontal velocity as did the work of Benjamin (1968), although he did not completely agree with von Kármán's methodology. The underlying consequence of this theory is that the Froude number and, thus, the advance velocity of the flow, is constant with downstream position. For this to be possible, mass conservation must exist in the structure such that mixing between it and the surrounding fluid is negligible, resulting in buoyancy preservation. Additionally, these works highlight the essential characteristic of this type of flow in that it is governed by buoyancy (Froude number dependence) and not the result of externally forced flows (Reynolds number dependence).

In later years, Simpson (1972, 1986) and Simpson and Britter (1979) were responsible for a large amount of work on smooth-surface gravity current flows. Much of their work has supported the observations and conclusions of earlier authors. Through salt-water modelling experiments, they clearly demonstrated that the head region of a gravity current is a zone of intense mixing. They were among the first to observe and define the two mechanisms, described in the previous section, by which lighter ambient fluid penetrates into the head region, i.e., 1) interfacial mixing due to shearing along the intruding head/ambient fluid boundary and 2) mixing due to the ingestion of lighter ambient fluid overrun by the head. They concluded that the second of these mechanisms plays a very minor role in the mixing of the gravity current head for smooth-surface flows. The gravitational instability of the lighter overrun fluid contributes only to the three-dimensionality of the smaller-scale sub-structure of the head (Simpson, 1972, 1986). Peters et al. (1997) showed that this second mechanism is very dependent on the scale of the surface roughness and contributes significantly to the mixing within the structure for flows over rougher surfaces.

The gravity current spread rate model developed by Keulegan, Benjamin and others assumed that the frontal velocity of the structure was constant, i.e., constant Froude number flow. In fact, this behaviour is characteristic of the first of two flow regimes identified by later authors such as Didden and Maxworthy (1982) and Huppert (1982). Real gravity current flows were shown to be governed by a balance of buoyant, inertial and viscous forces. During the early stages of the flow, the driving buoyant forces are exactly balanced by the inertial forces of the structure resulting in a constant velocity flow - the inertial/buoyant regime. As the flow progresses downstream, viscous shear stresses become much more significant, overtaking inertia as the dominant retarding force against buoyancy. This is the viscous/buoyant flow regime and is characterized by a decelerating advance velocity with downstream position.

It follows, then, that increased surface roughness over which the current flows should lead to increased shear stresses at the surface of contact. Consequently, flows over rougher surfaces should experience greater deceleration, and mixing, than equivalent flows over smooth surfaces. However, there has not been a substantial amount of work investigating gravity current flows over rougher surfaces. The bulk of the salt-water modelling work in this area has concentrated on flows that encounter single obstructions such as solid walls and porous fences (Rottman et al., 1985, Lane-Serf et al., 1995). Similar studies have been carried out in the wind tunnel with applications to HTAG dispersions (Ayrault et al., 1993, Havens et al., 1995). Unfortunately, very few publications have been found for flows over smaller-scale homogeneous roughness arrays such as used by the present authors. Petersen (1987), however, outlines much of the progress and research need for this area.

1.3 Laser-Induced Fluorescence Flow Visualization

Fluorescent dyes have been available for some time. The use of laser-induced fluorescence (LIF) for flow visualization, however, has only increased with the ability to easily generate thin light sheets of laser light. In many instances, LIF can provide significantly more valuable information about the anatomy of a fluid flow than can be acquired with conventional dye methods. This non-intrusive dye technique provides researchers with a simple and convenient flow marking scheme for measuring scalar quantities, such as concentration or temperature, within a flow. An extensive review of the theories of luminescence and fluorescence is given by Guilbault (1973) who points out that these measurement techniques are among the oldest and most established analytical methods available.

Walker (1987) performed an extensive examination of the behaviour of the fluorescent dye, fluorescein sodium. He looked at its emission intensity as a function of dye concentration and concluded that the emission signal responds linearly over a wide range of relatively low concentration values. His work, also, quantified the variation of the dye's emission signal strength with temperature, pH and excitation signal strength. He concluded that fluorescein sodium makes a good dye choice for LIF techniques but careful attention to control of conditions must be considered for its use.

Mapping of scalar properties such as species concentration, density or temperature in a planar field, or along a line, is the most frequently cited use of the LIF technique. Hesselink (1988) reports that LIF is a very useful tool in combustion research. Karasso and Mungal (1997) and Houcine et al. (1996) give descriptions of their uses of this technique to obtain instantaneous planar concentration profiles in various systems. Brungart et al. (1991) and Westblom and Svanberg (1985) describe similar uses of LIF for one-dimensional measurements along a line.

2. EXPERIMENTAL FACILITY AND METHODS

2.1 Overview of the Modelling, Visualization and Analysis Techniques

The salt-water modelling technique employed here uses a horizontal channel facility and two density-differentiated miscible fluids to generate small-scale, isothermal, adiabatic gravity current flows. The denser of the two fluids is continuously injected into a channel filled with the lighter fluid through an inlet located at the bottom of one end of the channel. The buoyancy-induced driving force that exists between the two fluids leads to a flow of the heavier fluid along the channel floor in the form of a gravity current.

LIF visualization is used in conjunction with the salt-water modelling method. Ths is a non-intrusive visualization technique in which a water-soluble fluorescent dye is used as a scalar flow marker. The dye emits a specific wavelength of visible light when excited by an appropriate wavelength of energy. In this work, fluorescein sodium dye is added to the more dense source fluid and, then, made to fluoresce by passing a sheet of argon ion laser light through the longitudinal mid-plane of the channel flow. The resulting two-dimensional planar views of the flow are sampled using video methods to provide images for further study. Digital image processing techniques are used to enhance the images and produce quantitative representations of the flows for comparison and evaluation purposes.

2.2 Water Channel System

The water channel facility consists of an open plexiglass channel, 240 cm long and 20 cm wide with a maximum possible channel fluid height of 30 cm. Saline fluid enters through an entry box section, 20 cm x 20 cm x 20 cm, located on the channel bottom at the upstream end. The entry box is filled with short sections of plastic pipe designed to promote a uniform velocity profile in the vertical entry flow. The saline fluid is injected vertically into the channel in this manner to ensure that no initial streamwise momentum is imparted to the gravity current flow. Additionally, with this method, a hydraulic jump does not form near the inlet so that the subsequent sub-critical flow is free of the strong turbulent entrainment associated with hydraulic jumps. The water channel system is shown schematically in Figure 3.

The height of the lighter channel ambient fluid is controlled by means of an adjustable overflow weir, located at the upstream end of the channel. As the more dense saline source fluid is injected into the entry box, ambient fluid is displaced over the weir. A horizontal splitter plate is fixed to the weir door, slightly below the spill edge, to separate the region of incoming dense fluid from that of the lighter overflowing fluid.

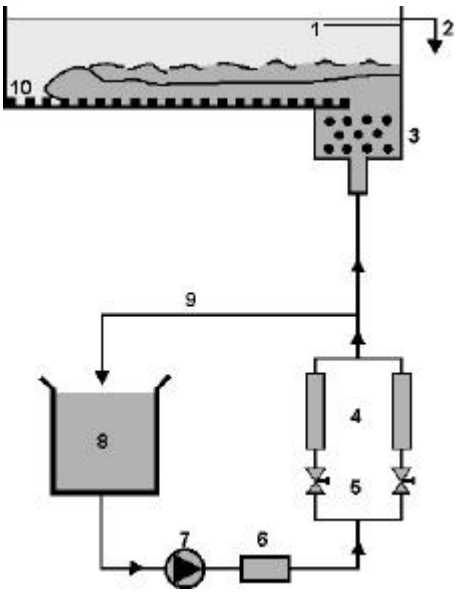

1. splitter plate
2. overflow weir
3. inlet entry box
4. flow meters
5. flow control valves
6. filter
7. circulating pump
8. saline storage reservoir
9. recirculation line
10. roughness array

Fig. 3. Schematic of the water channel and fluid circulation systems used to generate small-scale gravity current flows.

Square cross-section beams, fabricated from acrylic sheet, are used for the roughness elements. A surface roughness configuration consists of a two-dimensional array of these beams positioned on the channel floor, normal to the flow direction. The beams span the full channel width while the array extends over the full channel length. The first roughness element is positioned flush with the channel inlet edge. A two-dimensional configuration was chosen to minimize any three-dimensional, bulk motions in the flow.

For the present work, square elements with nominal side dimensions of 6, 13, 19 and 25 mm were used. These dimensions were chosen based on characteristic gravity current head and source layer heights observed in preliminary experiments. These were found to be approximately 50 mm and 25 mm, respectively, for the range of fluid density excesses used which yield a head/source layer height ratio of approximately two. This is in close agreement with the value of 2.16 proposed by Keulegan (1957, 1958). The roughness element heights, then, represent fractional values of the source fluid layer height of approximately 1, ¾, ½ and ¼. In all tests, beams were positioned with a downstream spacing equal to their width.

2.3 Fluid Circulation System

Typically, a two-fluid system of fresh/saline or saline/saline fluids is prepared using tap water. The less dense of the two fluids is used as the channel ambient fluid while the more dense fluid forms the gravity current. A commercial water softener salt (sodium chloride) is dissolved in one or both of the fluids to provide the required salinity difference. For the present experiments, source fluid density excesses of 0.01, 0.03 and 0.05 (1, 3 and 5%) were used where the source fluid density excess is defined as the excess density of the gravity current fluid above that of the ambient channel fluid. Over this range, the increase of kinematic viscosity of the fluid is negligible. To facilitate the LIF technique, it was necessary to buffer the working fluids to a pH above 8.

Saline solutions are prepared in 200 litre mixing/storage tanks by continuous circulation through a closed loop system (See Figure 3) which is isolated from the channel apparatus. Salt, in pellet form, is dissolved in a perforated bucket suspended in the solution. Circulation continues until the desired salinity is achieved and the solution is homogeneously mixed. If required, the pH buffering agent and/or fluorescent dye are added during this circulation process. An in–line filter removes any particles from the fluid. The less dense channel ambient fluid is prepared first and pumped into the channel. The channel is then isolated from the circulation system so that the more dense saline source fluid containing the fluorescent dye can be prepared. When this is complete and the channel ambient fluid has become quiescent, the heavier fluid is injected into the entry box slowly enough to minimize any mixing between the two fluids. When the saline source fluid level reaches the level of the channel floor, the injection is stopped and the fluids are allowed to become quiescent. Two variable area flow meters are used to control the source fluid injection rate.

2.4 Flow Illumination System

A Coherent Innova 70-4 argon ion laser is used to generate the laser beam required for the flow visualization technique. It has a rated power output of 4 W in the multi-line mode. In the single-line modes, the rated output power is 1.7 W for the green line (515nm) and 1.3 W for the blue line (488 nm). For the method reported here, the laser is operated in the blue line mode. The laser is combined with a fibre optic cable and probe assembly (Dantec 60X FibreFlow) which conveys the laser beam to the flow illumination system.

The laser sheet generating system is located above the flow channel and is shown schematically in Figure 4. The laser beam is reflected off a rotating front-surface mirror which rotates at a speed of 30,000 rpm. Consequently, the beam sweeps through the visualization section of the channel at a frequency of 500 Hz appearing to the naked eye as a two-dimensional sheet of light. Next, the resulting radially diverging laser sheet is passed through a large plano-cylindrical lens (162 mm radius and 74 mm centre thickness) to generate a vertically collimated light sheet. Two vertically separated thin slits are used to block out any unwanted reflections and scattered light from the excitation sheet to create a final vertical light sheet approximately 20 cm wide in the streamwise direction and 1.5 mm thick.

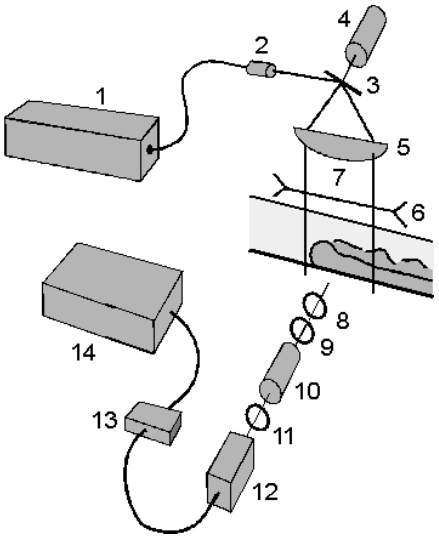

1. argon ion laser
2. fibre optics
3. scanning mirror
4. drive motor
5. collimating lens
6. slit assembly
7. excitation sheet
8. high-pass colour filter
9. 25 mm lens
10. image intensifier
11. 18 mm lens
12. video camera
13. time signal encoder
14. video recorder

Fig. 4. Schematic of the flow illumination and image acquisition systems used to visualize small-scale gravity currents.

As indicated previously, fluorescein sodium was selected for use in the LIF visualization technique employed here. With a quantum efficiency of approximately 90% (Guilbault, 1973), this dye's peak absorption wavelength of about 490 nm is well matched to the 488 nm excitation wavelength provided by the argon ion laser blue line. There is a sufficiently large separation between this absorption peak and that of the emission spectrum (515 nm) so that much of the excitation signal can be filtered out by appropriate optics without significantly reducing the strength of the emission signal to be measured. In addition to these characteristics, fluorescein sodium has other advantages over other fluorescent dyes such as the rhodamines. It is highly soluble in water and has a weak dependence on temperature, shown by Walker (1987) to be approximately 0.3% per EC. For the rhodamine dyes, this dependence is as much as 5% per EC (Guilbault, 1973).

For proper interpretation of the response of the dye, it is essential that 1) the dye emission signal strength be linearly proportional to both the dye concentration and the excitation signal strength and 2) the attenuation of the excitation signal be negligible as it passes through the dyed solution. According to Walker (1987), these conditions are typically satisfied for fluorescein sodium when the maximum dye concentration used is below approximately 10^{-7} mol/l or 0.040 mg/l for an excitation signal beam path length through the dyed fluid of approximately 10 cm. A series of tests were performed to determine the optimum maximum dye concentration to be used for the present technique so that each of these conditions would be satisfied. Accordingly, a maximum fluorescein sodium dye concentration of 5×10^{-8} mol/l or 0.020 mg/l was used.

As indicated, the strength of the emission signal for fluorescein sodium is strongly dependent on solution pH in the range from about 3 to 8. Walker (1987) shows that a 50% decrease in emission signal strength is observed for a drop in pH from about 8 to 6.5. Above a pH of 8, however, the emission signal strength is observed to be maximized and independent of the solution pH. Hence, all working fluids for these experiments were buffered with sodium hydroxide to a pH above 8.

Fluorescein sodium dye is, also, subject to two additional effects that can reduce the strength of the emission signal over time - oxidation and photo-decomposition (Guilbault, 1973). Oxidation is a chemical reaction fuelled by the oxygen dissolved in the working fluids while photo-decomposition results from exposure of the dyed solutions to the excitation signal or other background light sources. Two experiments were performed to quantify the degree by which the emission signal strength is affected by each of these conditions. They were performed in the water channel with a 10 cm layer of solution, buffered to a pH above 8 and homogeneously dyed at a concentration of 0.020 mg/l.

The first experiment looked at the variation of the signal strength over a six hour period due to oxidation. During this time, the dyed solution was not exposed to any light except during brief sampling times at 10 minute intervals so that the effects of photo-decomposition were not a factor. The dye emission signal strength was observed to fall gradually over the first 200 minutes after which the signal strength stabilized at about 77% of its initial value. Accordingly, it was concluded that aged dye solutions be used to avoid oxidation effects.

The second experiment was performed to quantify the photo-decomposition effects. This experiment used the aged dye solution that resulted from the previous experiment so that oxidation had already occurred. The solution was continuously exposed to a sheet of laser light at a fixed position in the water channel for a period of 25 minutes. Note that this time period is significantly longer than the one minute durations of a typical gravity current visualization experiment. The results showed that there was no further decrease in the emission signal strength due to photo-decomposition. It was concluded, then, that residual motion in the solution must act to replenish the dye in the laser sheet excitation region with fresh unexposed dye. Consequently, the turbulent nature of the gravity current flow should only enhance this effect so that dye particles have short exposure times and photo-decomposition becomes insignificant.

2.5 Image Acquisition System

Visualization of the gravity current flows was facilitated through the use of a black/white CCD video camera (Panasonic WV BD-400). In this manner, the experiments were sampled at a rate of 30 frames/second with a pixel resolution of 768x493. Since the excitation laser beam was scanned through the visualization section of the water channel at a rate (500 Hz) much greater than that of sampling (30 Hz), the dyed fluid it illuminate appeared as a two-dimensional light sheet to the camera. A S-VHS video cassette recorder (Panasonic AG-6720) was used to record the images for future processing and analysis. An external time signal encoder (For-A VTG-22) was used to superimpose a reference time signal on the recorded video signal.

As the image acquisition system is sensitive to light over the entire bandwidth of visible light, it was necessary to ensure that only the wavelength associated with the dye emission spectrum was sampled. Firstly, experiments were performed in a dark room to eliminate all background light noise. Secondly, a sharp cut-off, high-pass, Schott colour filter (Ealing OG-515) with 0% transmission at the excitation wavelength (490 nm) and 63% transmission at the emission wavelength (515 nm) was used to eliminate the excitation signal from the sampled signal. Since dye emission signal strengths are very low, a low-light level image intensifier (Astrolight 9100) was used to amplify the signal about four orders of magnitude. The video camera was coupled to the output display of the image intensifier (See Figure 4).

The image acquisition system (optics, image intensifier and camera) and flow illumination system (laser probe, rotating mirror and optics) were mounted on a traversing carriage that was able to be moved over the full channel length along two 13 mm diameter shafts located above each side of the channel. In this way, the traversing system could track the head of the gravity current flow as it progressed down the channel. To facilitate this, a computer control interface was developed to provide accurate control of the carriage position, velocity and elapsed traverse time.

2.6 Digital Image Processing System

A commercial frame grabbing board (Matrox MVP-AT/NP) and associated library of image processing routines were used to perform the digital processing for image enhancement and analysis. Processing was carried out at two levels. In the first level, real-time on-line processing was carried out on the video signal as the experiments were performed. The video signal

was digitized at 30 frames/second at a pixel resolution of 512x480. In this process, the image intensity was mapped to 256 discrete grey-levels ranging from black to white whereby each pixel in the image was assigned an intensity value based on its relative intensity in the image. Following this, low-level noise was removed from the signal while the image offset and gain were optimized. The output from this first processing level was, then, recorded using the S-VHS recorder and used as input to a more enhanced second level of processing.

This second level of image processing did not occur in real-time. Consequently, individual video frames were captured and stored to computer memory either as 1) single instantaneous snap-shots of the flow sampled with an exposure of 1/30 second or 2) single images that represent a time-average of a series of consecutive video frames. These individual images could, then, be subjected to more complex processing schemes for enhancement and analysis. For instance, a 3x3 neighbourhood averaging technique was applied to smooth the signal and eliminate much of the noise found in it. At this point, as well, pseudo-colour could be added, if desired, where a colour was assigned to a specific intensity range in the image.

Quantitative analysis of the images was carried out, in part, by extracting contour maps of image intensity. Since the relationship between the dye's emission signal strength and its concentration in the fluid is known to be linear, the image intensity field can easily be mapped to the dye concentration field. If it is assumed that the mass transport rates of the dye and of the salt in the solution are approximately the same, then, the dye concentration can act as a scalar marker for the salt concentration in the flow. The mass transport of each of these can occur by either molecular diffusion or turbulent mixing. In gravity current flows, however, turbulent mixing is far more significant than any diffusion process that might occur (Steckler et al., 1986). Consequently, it equally governs the transport of both the dye and salt throughout the gravity current structure. Additionally, the time scales associated with these flows are much too short for diffusion to be of any consequence.

Ultimately, this analysis produces concentration, or density, profiles of flow images that can be used to assess the mixing patterns. As shown in Figure 5, these maps highlight the areas where intense mixing occurs between the gravity current head structure and the surrounding ambient fluid. Statistical analysis of the images yields a mean head fluid density excess as well as parameters such as peak fluctuating density excess values and spatial standard deviations about the mean.

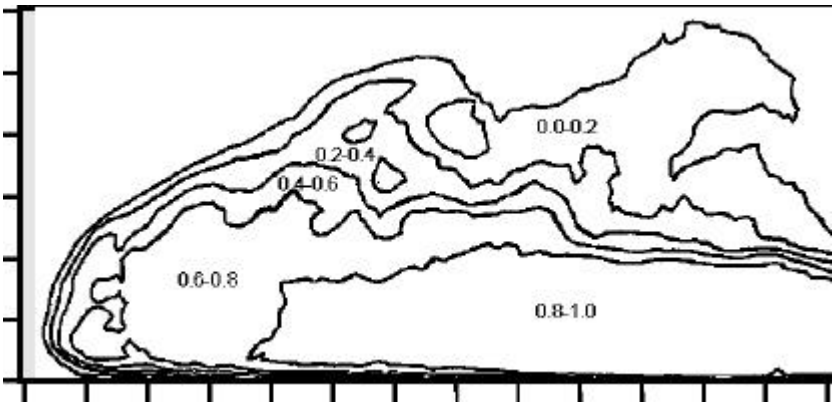

Fig. 5. Typical five-contour density profile map for the head of a gravity current flowing over a smooth surface with a 1% source fluid density excess. Scales shown are in 1 cm increments.

As indicated, time-averaged images could be acquired during the second level of image processing by averaging a series of consecutive images grabbed at a rate of 30 frames/second. However, as the time-averaging period is increased (i.e., number of images to be averaged), the shorter time-scale features of the flow are not captured as shown in Figure 6. This may not be desirable so it was necessary to optimize the time-averaging period to reduce noise levels while maintaining a useful level of flow detail. It was shown that increasing this averaging period significantly reduces the spatial standard deviation in the emission signal strength measurements without reducing the overall mean intensity level in the sampled images. Accordingly, a one second (30 frame) time-averaging period was used for acquisition of all time-averaged images.

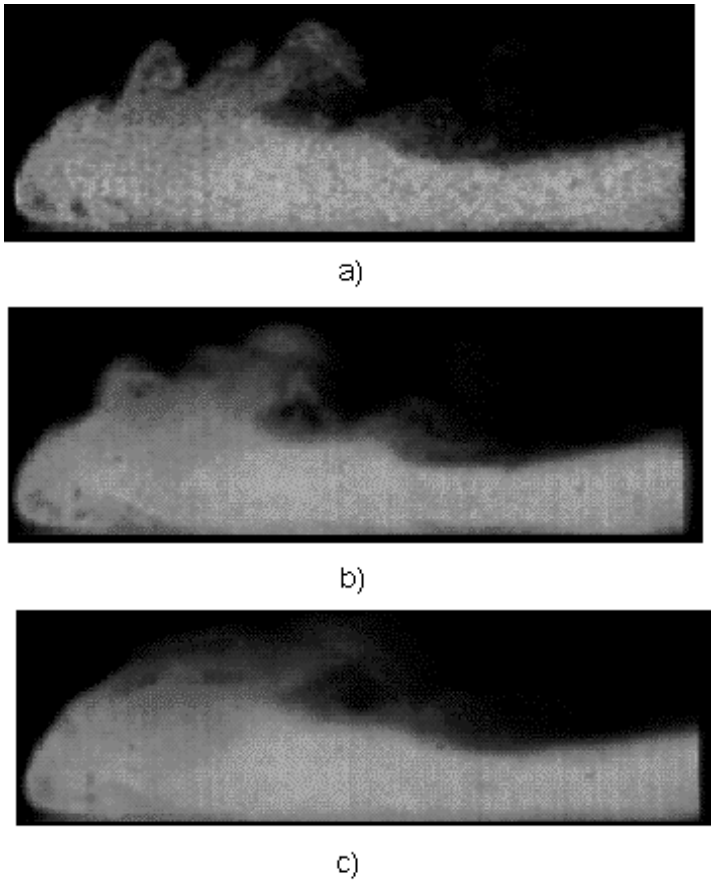

Fig. 6. Gravity current images that illustrate the effect of time averaging on the image detail for a) a single snapshot, b) a 10 frame average and c) a 30 frame average.

3. SUMMARY OF EXPERIMENTS

Three series of tests were performed in a water channel facility designed to examine gravity current flows in which the source fluid density excess, $)\Delta/\Delta_S$ (subscript $_S$ refers to the source fluid) for each test series was 1, 3 and 5%. Source injection flow rates per unit channel width, Q, of 10.3, 10.6 and 10.8 cm ^{2}/s, corresponding to the above source fluid density excesses, were used to generate flows with source buoyancy fluxes, B_S, of 101, 312 and 530 cm ^{3}/s^3, respectively. The source buoyancy flux is given as $g(\ )\Delta/\Delta_S)Q$ where g is the acceleration due to gravity. Based on these numbers, the turbulence levels of the resulting gravity currents were high enough to ensure Reynolds number independence as first observed by Schmidt (1911). In each test, the height of the lighter ambient fluid in the channel was 30 cm.

As previously indicated, five surface roughness conditions were examined for each of the three values of fluid density excess considered, yielding a total of fifteen tests. These included a smooth-surface condition for each test series which provided a base case against which the rough-surface flow results could be compared. The roughness arrays consisted of square-beam elements, 6, 13, 19 and 25 mm on a side, installed as previously described.

4. RESULTS AND GENERAL CONCLUSIONS

The techniques of salt-water modelling, laser-induced fluorescence and digital image processing were successfully used to model, visualize and analyze small-scale, two-dimensional, continuous source gravity current flows. It has been shown that the facility and experimental techniques developed can successfully provide full-field, two-dimensional planar images of the flow structure for qualitative and quantitative study. These images can be used to study the downstream spread rate and mixing associated with rough-surface gravity current flows.

The following general conclusions were drawn with respect to the visualization techniques employed.

1) Fluorescein sodium is a suitable fluorescent dye for use in the LIF visualization technique.
2) A maximum dye concentration of 5×10^{-8} mol/l should be used to ensure proper dye response.
3) To maximize the emission signal strength, it is necessary to buffer the working fluids to a pH above 8.
4) Aged dye solutions should be used to minimize the effects of oxidation and photo-decomposition.
5) A time-averaging period of one second (30 frames) should be used to produce images for analysis.

The experimental methods showed that the smooth-surface gravity current flows generated in this study behaved consistently with the accepted theory and observations in terms of structure, flow dynamics and mixing behaviour for the range of source fluid density excess considered. These results, therefore, validate the techniques developed and provide valuable reference cases for evaluation of the rough-surface flows. In all smooth-surface tests, the downstream spreading of the flows was governed initially by the inertial/buoyant (constant frontal velocity) model with transition to the viscous/buoyant (decelerating flow) model occurring where expected. Additionally, in each smooth-surface case, it was confirmed that the overall downstream dilution of the gravity current head is negligible for the inertial/buoyant flow regime as assumed in the spread rate model for this type of flow.

Comparison of the rough-surface flow results with those of the smooth-surface tests confirmed that the accepted smooth-surface flow models do not extend very well to the rough-surface flows considered here. Generally, when compared to the smooth-surface tests, the influence of the rougher surfaces produced gravity current flows that 1) exhibited a lower initial constant frontal advance velocity in the inertial/buoyant flow regime, 2) were dominated by viscous effects much earlier in the flow and 3) decelerated at much greater rates in the viscous/buoyant regime.

These effects were attributed to two interactions between the gravity current, the ambient fluid and the solid boundary condition. Firstly, a significant volume of lighter ambient fluid, trapped in the roughness element spaces, was able to be entrained into the heavier head structure as it moved over the roughness array. This effect produced an additional dilution of the head, not experienced in the smooth-surface flows, that resulted in a weaker buoyant driving force and, thus, a lower advance velocity over the entire channel length. This is a magnified case of the second mixing mechanism described in Section 1.2. Secondly, increased shear stresses at the lower surface boundary, due to the larger roughness scales, promoted an earlier transition to the viscous/buoyant flow regime, characterized by a significant deceleration of the flow.

Consequently, the existing smooth-surface theory was modified to produce a new rough-surface gravity current flow model. It incorporates 1) an appropriate rough-surface entrainment factor to account for the additional head dilution brought on by the mixing with the ambient fluid trapped between the roughness elements and 2) a wall shear stress model based on a modified or effective fluid viscosity approach (Nikuradse, 1933, Schlichting, 1979, Coleman et al., 1984) to account for the increased surface friction of the roughness elements. Using this method, modified spread rate equations for both the inertial/buoyant and viscous/buoyant flow regimes were developed that are applicable for both the smooth-surface and rough-surface flows considered here.

Following this concept, the spread rate data for all tests are presented in Figure 7 in which the normalized frontal velocity (Froude number) is plotted against the normalized downstream position. The figure shows that the modified spread rate equations adequately represent all test results. Over the downstream extent, both the inertial/buoyant (constant frontal velocity) and viscous/buoyant (decelerating flow) regimes are evident. Figure 8 shows the effect of the surface roughness scale on the amount of mixing in the gravity current head. Here, a mixing ratio was defined to quantify the amount of mixing in a rough-surface flow compared to that in a smooth-surface flow with the same conditions. In addition to the expected increase in mixing with larger roughness scales, the results show that the dilution rate, also, increases with a larger source fluid density excess for a given surface roughness condition. This can be attributed to the greater tendency for the heavier flows to fill the spaces between the roughness elements as they are passed over, forcing the lighter fluid trapped between them out to be mixed in the head.

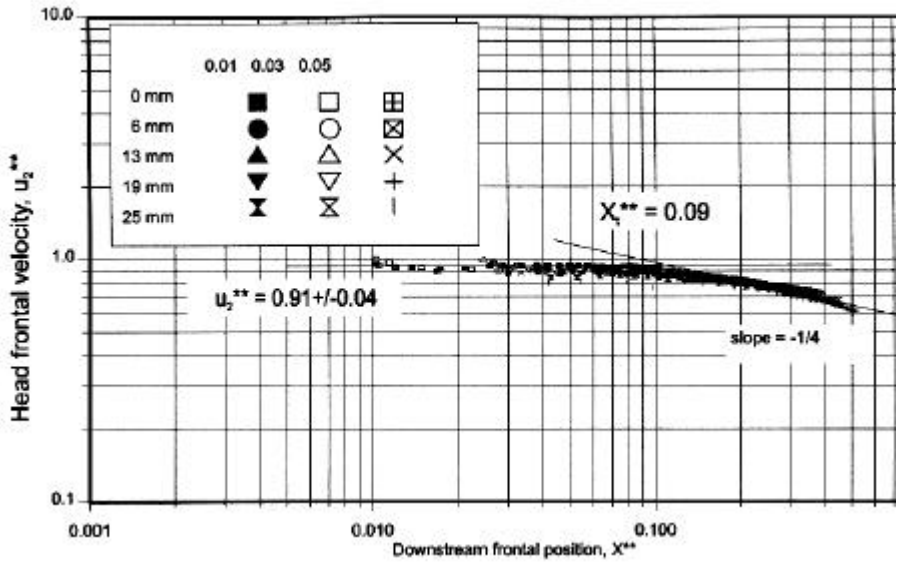

Fig. 7. Head frontal velocity versus downstream position for all gravity current flows over the range of surface roughness scale and source fluid density excess used.

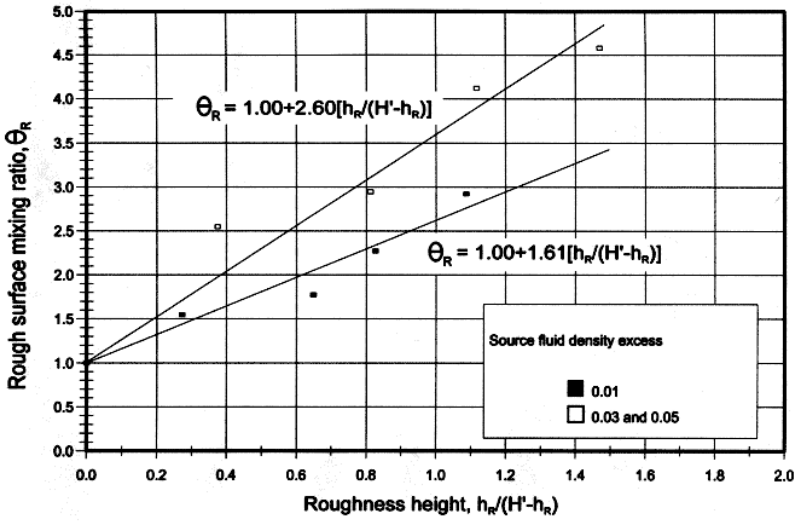

Fig. 8. Influence of the surface roughness scale on the rough-surface mixing ratio for flows with 1, 3 and 5% source fluid density excesses.

REFERENCES

Ayrault, M., Simoens, S. and Mejean, P. (1993). “Effects of a two-dimensional obstacle on the dispersion of dense gas releases”, Symp.Experimental and Numerical Flow Visualization, ASME Winter Annual Meeting, New Orleans, Louisiana, FED-Vol 172, pp. 233-239.

Benjamin, T.B. (1968). "Gravity Currents and Related Phenomena", J. Fluid Mechanics, Vol. 31, Part 2, pp. 209-248.

Brungart, T.A., Petrie, H.L., Harbison, W.L. and Merkle, C.L. (1991). "A Fluorescence Technique for Measurement of Slot Injected Fluid Concentration Profiles in a Turbulent Boundary Layer", Exp. Fluids, Vol. 11, pp. 9-16.

Coleman, H.W., Hodge, B.K. and Taylor, R.P. (1984). “A re-evaluation of Schlichting’s surface roughness experiment”, J. Fluids Engineering, Vol. 106, pp. 60-65.

Didden, N. and Maxworthy, T. (1982). “The viscous spreading of plane and axisymmetric gravity currents”, J. Fluid Mechanics, Vol. 121, pp. 27-42.

Guilbault, G.G. (1973). Practical Fluorescence: Theory, Methods and Techniques , Marcel Dekker, Inc., N.Y. 664 p.

Havens, J.A., Spicer, T.O., Walker, H. and Williams, T. (1995). “Validation of mathematical models using wind-tunnel data sets for dense gas dispersion in the presence of obstacles”, Loss Prevention and Safety Promotion in the Process Industries, Proc. 8 th Int. Symp., Antwerp, Belgium, June 6-9, pp. 171-184.

Huppert, H.E. (1982). “The propagation of two-dimensional and axisymmetric viscous gravity currents over a rigid horizontal surface”, J. Fluid Mechanics, Vol. 121, pp. 43-58.

Hesselink, L. (1988). "Digital Image Processing Flow Visualization", Ann. Rev. Fluid Mechanics, Vol. 20, pp. 421-485.

Houcine, I., Vivier, H., Plasari, R. and Villermaux, J. (1996). “Planar laser induced fluorescence technique for measurements of concentration fields in continuous stirred reactor tanks”, Exp. Fluids, Vol. 22, pp. 95-102.

Karasso, P.S. and Mungal, M.G. (1997). “PLIF measurements in aqueous flows using the ND:YAG laser”, Exp. Fluids, Vol. 23, pp. 382-387.

Keulegan, G.H. (1957). "An Experimental Study of the Motion of Saline Water from Locks into Fresh Water Channels", National Bureau of Standards, U.S. Department of Commerce, Washington, D.C., Report # 5168.

Keulegan, G.H. (1958) "The Motion of Saline Fronts in Still Water", National Bureau of Standards,U.S. Department of Commerce, Washington, D.C., Report # 5831.

Lane-Serf, G.F., Beal, L.M. and Hadfield, T.D. (1995). “Gravity current flows over obstacles”, J. Fluid Mechanics, Vol. 292, pp. 39-53.

Nikuradse, J. (1933). "Strömungsgesetze in rauhen Rohren", V.D.I. Forschungsheft, No. 361.

Peters, W.D., Cogswell, S.R. and Venart, J.E.S. (1997). “Mixing in gravity current heads flowing over rough surfaces”, Developments in Laser Techniques and Fluid Mechanics , Eds.: R.J. Adrian et al., Springer, Berlin, Ch. III, pp. 325-339.

Petersen, R.L. (1987). "Surface Roughness Effects on Heavier-Than-Air Gas Diffusion", American Petroleum Institute, Washington, D.C., API Publication No. 4459, 44 p.

Rottman, J.W., Simpson, J.E., Hunt, J.C.R. and Britter, R.E. (1985). “Unsteady gravity current flows over obstacles: Some observations and analysis related to the Phase II trials”, J. Hazardous Materials, Vol. 11, pp. 325-340.

Schlichting, H. (1979). Boundary Layer Theory, McGraw-Hill, New York, 619 p.

Schmidt, W. (1911). "Zer Mechanik der Boen", Z. Meteorol, Vol. 28, pp. 355-362.

Simpson, J.E. (1972). "Effects of the Lower Boundary on the Head of a Gravity Current," J. Fluid Mechanics, Vol. 53, Part 4, pp. 759-768.

Simpson, J.E. (1986). "Mixing at the Front of a Gravity Current", Acta Mechanica, Vol. 63, pp. 245 -253.

Simpson, J.E., and Britter, R.E. (1979). "The Dynamics of the Head of a Gravity Current Advancing Over a Horizontal Surface", J. Fluid Mechanics, Vol. 94, Part 3, pp. 477 -495.

Steckler, K.D., Baum, H.R., and Quintiere, T.G. (1986). "Salt Water Modeling of Fire Induced Flows in Multicompartment Fires", Twenty-First Symp.Combustion, The Combustion Institute, pp. 143-149.

von Kármán, T. (1940). "The Engineer Grapples with Nonlinear Problems", Bulletin of the American Mathematical Society, Vol. 46, pp. 615-683.

Walker, D.A. (1987). "A Fluorescence Technique for Measurement of Concentration in Mixing Fluids", J. Physics, E, Scientific Instruments, Vol. 20, pp. 217-224.

Westblom, U. and Svanberg, S. (1985). “Imaging measurements of flow velocities using laser-induced fluorescence”, Physica Scripta, Vol. 31, pp. 402-405.